



CHORUS

This is the accepted manuscript made available via CHORUS. The article has been published as:

Smearred nematic quantum phase transitions due to rare-region effects in inhomogeneous systems

Tianbai Cui and Rafael M. Fernandes

Phys. Rev. B **98**, 085117 — Published 8 August 2018

DOI: [10.1103/PhysRevB.98.085117](https://doi.org/10.1103/PhysRevB.98.085117)

Smearred nematic quantum phase transitions due to rare-region effects in inhomogeneous systems

Tianbai Cui and Rafael M. Fernandes

School of Physics and Astronomy, University of Minnesota, Minneapolis, MN 55455, USA

The concept of a vestigial nematic order emerging from a “mother” spin or charge density-wave state has been applied to describe the phase diagrams of several systems, including unconventional superconductors. In a perfectly clean system, the two orders appear simultaneously via a first-order quantum phase transition, implying the absence of quantum criticality. Here, we investigate how this behavior is affected by impurity-free droplets that are naturally present in inhomogeneous systems. Due to their quantum dynamics, finite-size droplets sustain long-range nematic order but not long-range density-wave order. Interestingly, rare droplets with moderately large sizes undergo a second-order nematic transition even before the first-order quantum transition of the clean system. This gives rise to an extended regime of inhomogeneous nematic order, which is followed by a density-wave quantum Griffiths phase. As a result, a smearred quantum nematic transition, separated from the density-wave quantum transition, emerges in moderately disordered systems.

I. INTRODUCTION

In an electronic nematic phase, the crystalline point group symmetry is lowered by electronic degrees of freedom^{1–3}. In analogy to liquid crystals, it can arise via the partial melting of a translational symmetry-breaking smectic phase, which in electronic systems corresponds to a spin or charge density-wave (DW). In several materials, the DW can have multiple wave-vectors \mathbf{Q} related by the symmetries of the underlying lattice. A well known example is a DW on a square lattice with possible ordering vectors $(Q, 0)$ and $(0, Q)$, related by tetragonal symmetry. In these cases, upon melting the DW, the system may form a vestigial Ising-nematic phase in which the translational symmetry of the lattice is preserved, but its rotational symmetry is broken. In the above example on the square lattice, the nematic transition lowers the tetragonal symmetry down to orthorhombic.

Such a mechanism for electronic nematicity has been proposed in both iron-based superconductors^{4–6}, in which the DW is in the spin channel, and in the high- T_c cuprates^{1,7–9}, where the DW can be in both spin and charge channels. Interestingly, both materials at optimal doping exhibit behavior characteristic of a quantum critical point, such as strange metallicity and enhancement of the quasiparticle effective mass^{10–12}. This has motivated deeper investigations of quantum nematic phase transitions in metals, in order to elucidate whether a putative nematic quantum critical point is a key ingredient of the phase diagrams of these superconducting compounds¹³.

Several theoretical works have shown that, for a perfectly clean quasi-two-dimensional metallic system, the vestigial Ising-nematic order and the mother density-wave order undergo a simultaneous $T = 0$ first-order transition, implying the inexistence of a quantum critical point^{6,14–16}. However, disorder, ubiquitously present in realistic systems, can have dramatic effects on quantum phase transitions^{3,17–26}. Thus, in order to assess the relevance of nematicity to the properties of these compounds,

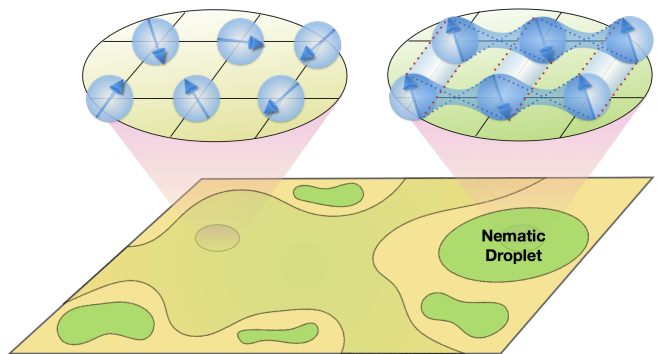


Figure 1. Illustration of a moderately diluted system displaying an infinite cluster (light green) and finite-size droplets (dark green) devoid of impurities. For this illustration, we consider a “mother” spin-density wave and its vestigial Ising-nematic phase. At $T = 0$, finite-size droplets cannot sustain long-range spin order (indicated by the disordered spins in the inset), but they can support long-range nematic order (indicated by the different spin-spin correlations along the x and y axis, resulting in unequal x and y bonds). Importantly, droplets of moderate sizes undergo a second-order nematic transition even before the bulk system (and thus the infinite cluster) undergoes its simultaneous first-order density-wave and nematic transition.

it is paramount to understand the interplay between disorder and nematic order. Previous works have focused mostly on non-vestigial Ising-nematic phases^{27–29}, including the role of Griffiths effects³⁰, and on random-field or random-mass types of disorder in the DW degrees of freedom^{31,32}.

In this paper, we investigate the impact of rare regions on the vestigial Ising-nematic order arising from a DW quantum phase transition. A rare region is a relatively large droplet that is devoid of impurities in a disordered system (see Fig. 1). For our purposes, we consider point-like, randomly diluted impurities that completely suppress nematic and DW orders locally. Al-

though the probability of finding such droplets decreases exponentially with their size, their impact on phase transitions can be significant, causing Griffiths singularities in thermodynamic quantities^{33,34} or smearing phase transitions³⁵. These effects are particularly strong near a quantum phase transition, due to the fact that the impurity at $T = 0$ is perfectly correlated along the “time” axis^{21,36}.

As we show here, the rare regions completely change the nature of the simultaneous first-order nematic-DW quantum transition in a two-dimensional itinerant system. This is because of the crucial role of the droplet’s dissipative quantum dynamics^{37–39}, which allows long-range Ising-nematic order in finite-size droplets at $T = 0$ (see also Ref. 19), but not DW order (for spin or incommensurate charge density-waves). By performing large- N calculations on a finite-size droplet, we find a wide parameter range for which the first droplets to order nematically at $T = 0$ are not the largest ones, but the droplets of moderately large sizes. Remarkably, while the *largest droplets* undergo a *first-order* nematic transition very close to the quantum phase transition of the clean system, the droplets of *moderate sizes* undergo a *second-order* nematic transition even before the clean system orders. The result is the emergence of an inhomogeneously ordered nematic phase, characteristic of a smeared nematic quantum phase transition^{21,38}, in the regime where the clean system is not ordered. Our findings, illustrated in Fig. 2, indicate also that a DW Griffiths phase appears inside this inhomogeneous nematic state, preceding the onset of long-range DW and homogeneous nematic order. As we argue below, this behavior may be related to recent puzzling experimental observations in iron-based compounds.

II. LOW-ENERGY MODEL

We consider a general two-dimensional low-energy model that yields vestigial Ising-nematic order from a mother DW phase on the square lattice. For concreteness, we consider two N -component DW order parameters, Δ_X and Δ_Y , corresponding to two wave-vectors $\mathbf{Q}_X = (Q, 0)$ and $\mathbf{Q}_Y = (0, Q)$ related by tetragonal symmetry. In the case of spin density-wave, $N = 3$ (commensurate) or $N = 6$ (incommensurate), whereas for charge density-wave, $N = 1$ (commensurate) or $N = 2$ (incommensurate). Hereafter, we consider only the case $N > 1$, as relevant for copper-based and iron-based superconductors. The low-energy action is given by:⁶

$$S[\Delta_X, \Delta_Y] = \int_{\mathbf{q}, \omega} \left[\chi_{\mathbf{q}, \omega}^{-1} (\Delta_X^2 + \Delta_Y^2) + \frac{u}{2} (\Delta_X^2 + \Delta_Y^2)^2 - \frac{g}{2} (\Delta_X^2 - \Delta_Y^2)^2 \right] \quad (1)$$

where $\int_{\mathbf{q}, \omega} = \int \frac{d^d q}{(2\pi)^d} \int \frac{d\omega}{2\pi}$. Here, $\chi_{\mathbf{q}, \omega}^{-1} = r_0 + \mathbf{q}^2 + \gamma |\omega|^{2/z}$ is the inverse DW susceptibility, with the “tuning parameter” r_0 denoting the distance to the mean-field quantum

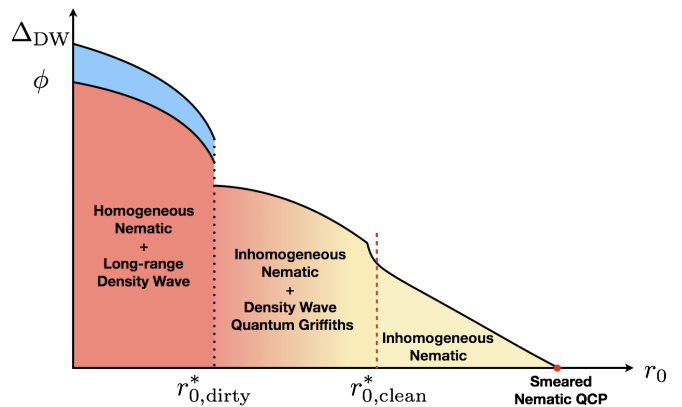


Figure 2. Schematic phase diagram illustrating our main results. Here, r_0 is a control parameter, such as doping or pressure. In the clean system at $T = 0$, the nematic (ϕ) and density-wave (Δ_{DW}) order parameters appear simultaneously at $r_{0,\text{clean}}^*$ (dashed line). In the moderately diluted system, which still has a percolating (infinite) cluster, the first-order quantum transition is expected to be suppressed down to $r_{0,\text{dirty}}^*$ (dotted line). For $r_0 > r_{0,\text{clean}}^*$, moderately large droplets undergo a second-order nematic transition, giving rise to inhomogeneous nematic order. For $r_{0,\text{dirty}}^* < r_0 < r_{0,\text{clean}}^*$, exponentially large droplets have an exponentially large DW correlation length, resulting in a DW quantum Griffiths phase. Whether ϕ jumps or continuously evolves at $r_{0,\text{dirty}}^*$ depends on details of the disorder distribution.

phase transition. For itinerant systems, the dynamical critical exponent is $z = 2$ and γ is the Landau damping coefficient. Vestigial Ising-nematic order arises when $g > 0$. Physically, the emergent Ising-nematic order parameter $\langle \phi \rangle = g \langle \Delta_X^2 - \Delta_Y^2 \rangle$, which can onset before the DW, corresponds to unequal fluctuations around the two DW wave-vectors. Mathematically, it is obtained by performing a Hubbard-Stratonovich transformation of the second quartic term of Eq. (1):

$$S_{\text{eff}} = \int_{\mathbf{q}, \omega} \left\{ \frac{\phi^2}{2g} - \frac{\psi^2}{2u} + \frac{N}{2} \ln \left[(\chi_{\mathbf{q}, \omega}^{-1} + \psi)^2 - \phi^2 \right] \right\} \quad (2)$$

To obtain this effective action, we also performed a Hubbard-Stratonovich transformation of the first quartic term of Eq. (1) to introduce the Gaussian-fluctuations field $\langle \psi \rangle = u \langle \Delta_X^2 + \Delta_Y^2 \rangle$. In the large- N limit, and after rescaling the quartic coefficients $(u, g) \rightarrow (u, g)/N$, the equilibrium values of ϕ and ψ as function of r_0 can be found within the saddle-point approximation $\frac{\delta S_{\text{eff}}}{\delta \psi} = \frac{\delta S_{\text{eff}}}{\delta \phi} = 0$. Note that $r_0 + \psi = |\phi|$ indicates an instability towards the DW phase, whereas $\phi \neq 0$ indicates an instability towards the Ising-nematic phase. For $d = 2$, the two transitions are split at finite temperatures, but merge into a single first-order transition at $T = 0$ (see Fig. 2). These large- N results, reproduced in the Appendix, were obtained before⁶ and confirmed by renormalization group analysis^{14–16}.

III. LARGE- N SOLUTION FOR A SINGLE DROPLET

To assess the relevance of rare regions to the nematic and DW quantum phase transitions, we first solve the large- N saddle-point equations for a single droplet of linear size L , and later average over the distribution of droplets. The strategy is similar to that employed in Ref. 36 to study Griffiths effects near a metallic anti-ferromagnetic quantum critical point. Due to the finite size of the droplet, the momentum integration in Eq. (2) is replaced by a discrete sum over momenta $\mathbf{q} = \frac{2\pi}{L}\mathbf{n}$, with $\mathbf{n} = (n_x, n_y)$ and $n_{x,y}$ integer. The saddle-point equations at $T = 0$ become (details in Appendix A):

$$r = r_0 - ur \left(\ln \frac{\Lambda^2}{\sqrt{r^2 - \phi^2}} + 1 - \frac{\phi}{r} \tanh^{-1} \frac{\phi}{r} \right) + \frac{2\pi u}{L^2} \{ \mathcal{F}[(r - \phi)L^2] + \mathcal{F}[(r + \phi)L^2] \} \quad (3)$$

$$\phi = \phi g \left(\ln \frac{\Lambda^2}{\sqrt{r^2 - \phi^2}} + 1 - \frac{r}{\phi} \tanh^{-1} \frac{\phi}{r} \right) + \frac{2\pi g}{L^2} \{ \mathcal{F}[(r - \phi)L^2] - \mathcal{F}[(r + \phi)L^2] \} \quad (4)$$

where $r = r_0 + \psi$ is proportional to the inverse squared DW correlation length, $r_0 \rightarrow r_0 + u \int_{\mathbf{q}, \omega} \frac{1}{q^2 + \gamma|\omega|}$ is the renormalized distance to the DW quantum critical point, and Λ is the momentum cutoff, hereafter set to be $1/a$ (a is the lattice parameter). Note that the quartic coefficients have been rescaled by $u \rightarrow u/(4N\pi^2\gamma)$ and $g \rightarrow g/(4N\pi^2\gamma)$. The droplet finite-size effects are encoded in the function $\mathcal{F}(y) = \frac{1}{\pi} \sum_{\mathbf{n} \neq \mathbf{0}} \frac{\sqrt{y}}{|\mathbf{n}|} K_1(|\mathbf{n}|\sqrt{y})$, where $K_1(x)$ is the modified Bessel function of the second kind. Because $\mathcal{F}(y \gg 1) \sim y^{1/4} e^{-\sqrt{y}}$, Eqs. (3)-(4) recover the saddle-point expressions for the infinite system $L \rightarrow \infty$.

To understand how the finite size of the droplet affects the DW and nematic transitions, we recall that the DW transition takes place when $r = |\phi|$. But because $\mathcal{F}(y \ll 1) \sim -\ln y$, there is no solution to Eqs. (3)-(4) with $r = |\phi|$. This is a consequence of Mermin-Wagner theorem: at $T = 0$, the finite-size droplet has an effective dimensionality $d_{\text{eff}} = z = 2$, which is the lower critical dimension for the DW transition³⁶.

The situation is completely different for the Ising-nematic transition: since its lower critical dimension $d_c = 1 < d_{\text{eff}}$, long-range Ising-nematic order can onset at $T = 0$ even in a droplet of finite size L ^{19,38}. To address which droplets order first, and the character of the Ising-nematic transition inside them, we solved Eqs. (3)-(4) to obtain $\phi(r_0, L)$. The results are shown in Fig. 3; for comparison, we also show the first-order behavior of the nematic order parameter of the clean system, $\phi_{\text{clean}} \equiv \phi(L \rightarrow \infty)$, which orders at $r_{0,\text{clean}}^* \equiv r_0^*(L \rightarrow \infty)$.

The figure illustrates two very different behaviors: droplets of moderately large sizes display a non-zero ne-

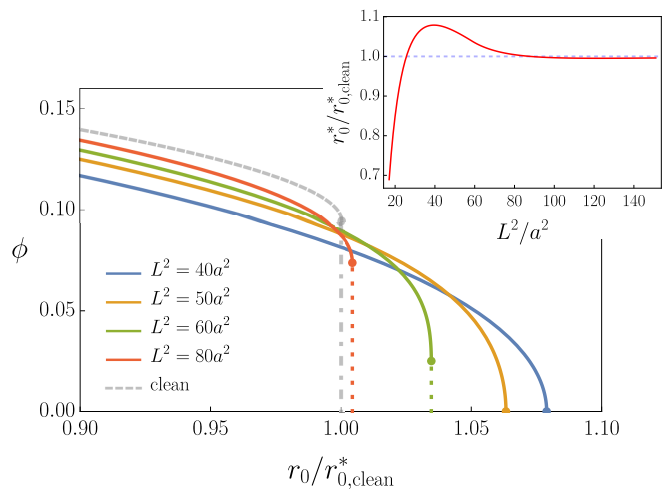


Figure 3. Nematic order parameter ϕ (in units of Λ^2) inside a droplet of “volume” L^2 , as a function of the control parameter r_0 (in units of the value $r_{0,\text{clean}}^*$ for which the clean system undergoes the first-order nematic transition). $\phi_{\text{clean}} \equiv \phi(L \rightarrow \infty)$ is shown as a dashed line. First-order transitions are indicated by the dotted line. The inset shows the value of the tuning parameter r_0^* at the nematic transition inside a droplet as function of the droplet volume L^2 .

matic order parameter already in the non-ordered phase of the clean system, i.e. the nematic transition inside these droplets happens at $r_0^*(L) > r_{0,\text{clean}}^*$. Importantly, the nematic transition in these droplets is generally second-order. In contrast, large droplets undergo a first-order nematic transition very close to the clean phase transition, i.e. $r_0^*(L) \approx r_{0,\text{clean}}^*$. Note that small droplets (not shown) only order below $r_{0,\text{clean}}^*$. This is more clearly seen in the inset, which shows the nematic transition parameter $r_0^*(L)$ as function of the size L . For the particular values of u and g used here, $u = 0.9$ and $g = 0.25u$, the first droplet to order has “volume” $L^2 \approx 40a^2$, and all droplets with volumes smaller than $L^2 = 58a^2$ undergo a second-order nematic transition. As we show in Appendix B, this behavior is not specific to these values of u and g , but happen in a wide region of the (u, g) parameter space. Importantly, for all droplets, the DW transition does not take place, i.e. the nematic and DW quantum phase transitions are naturally split inside a finite-size droplet.

IV. AVERAGE OVER DROPLETS

To assess the impact of the nematically ordered droplets on the thermodynamic properties of the system, we need to average over the different possible droplets. The key quantity is thus the probability $P(V)$ of a impurity-free droplet of volume $V \equiv L^2$ being realized in the system, which is determined by the disorder distribution. For concreteness, we consider random dilutions that kill DW and nematic order at a given site with

probability $1 - p$, such that $p = 0$ ($p = 1$) corresponds to the completely dirty (clean) system. Using results of percolation theory⁴⁰, we can write down the approximate expression (see Appendix C for details):

$$P(V) = \frac{p_c V^{1-\tau} \exp(-V/V_0)}{\sum V^{1-\tau} \exp(-V/V_0)} \quad (5)$$

Here, $\tau = 187/91$ is a critical exponent, V_0 is the typical volume of an impurity-free droplet for a given p , and p_c is the percolation threshold for clean sites. Because V_0 changes from 0 to ∞ from $p = 0, 1$ to the percolation threshold $p = p_c$, we treat V_0 as our disorder “tuning parameter,” instead of p .

We consider here the case where dilution is moderate, and the system is above the percolating threshold for clean sites, $p > p_c$. In this case, in addition to the finite-size droplets described above, there is a single infinite percolating droplet devoid of impurities, which behaves similarly to the clean bulk system (see schematic Fig. 1). Because the infinite droplet has less sites than the bulk system, the DW-nematic first-order transition inside of it is expected to happen for $r_{0,\text{dirty}}^* < r_{0,\text{clean}}^*$. Thus, for $r_0 > r_{0,\text{dirty}}^*$, the average Ising-nematic order parameter is given solely by the contributions from the finite-size droplets, $\bar{\phi} = \sum P(V) \phi(V) dV$. We tacitly assume that there is a very weak inter-droplet interaction – for instance mediated by the lattice – that align the Ising-nematic order parameters of different droplets.

The results for $\bar{\phi}$ are shown in Fig. 4 for different values of V_0 . Because the first droplets to order have moderate sizes and undergo a second-order transition, $\bar{\phi}$ seems to evolve continuously as function of r_0 . Our numerical result suggests a kink of $\bar{\phi}$ at $r_{0,\text{clean}}^*$, although a small jump might also be possible. This behavior is a consequence of the fact that most of the large droplets order very close to $r_{0,\text{clean}}^*$ (see inset of Fig. 3). At $r_{0,\text{dirty}}^*$, $\bar{\phi}$ acquires the additional contribution from the infinite droplet. At this point, the resulting nematic order parameter can then either undergo a meta-nematic transition, in which it jumps between two non-zero values, or display another kink in a continuous fashion. The ultimate behavior is determined by details of the disorder distribution beyond the scope of our model.

The proliferation of moderate-size droplets sustaining long-range nematic order upon approaching the clean DW-nematic quantum phase transition at $r_{0,\text{clean}}^*$ signals the emergence of an inhomogeneously ordered nematic state separated from the DW transition. The resulting phase transition is thus a smeared quantum phase transition. The smeared nematic quantum phase transition discovered here is very different than the smeared transitions discussed previously in other contexts^{21,35,38} (for a review, see Ref. 41?). First, in our case, many finite-size droplets order even before the clean system. Second, the droplets that order first are not the largest ones, but the droplets of intermediate size. This ensures the existence of a well-defined critical point, regardless of whether the

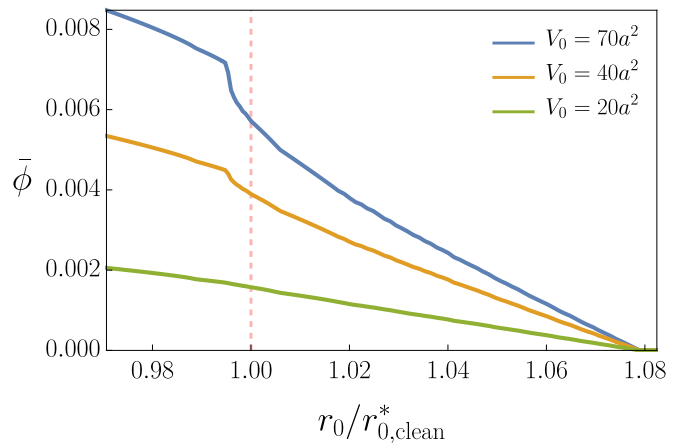


Figure 4. Average nematic order parameter of all droplets, $\bar{\phi}$ (in units of Λ^2), as function of the control parameter, r_0 (in units of $r_{0,\text{clean}}^*$). Different curves correspond to different “critical” droplet volumes V_0 associated with the probability distribution (5).

disorder distribution is bounded or not. Finally, the size of the droplets determines not only when they order, but also the character of the corresponding phase transition (i.e. second- or first-order). As for the DW order, it only onsets at $r_{0,\text{dirty}}^*$, since finite-size droplets cannot sustain DW long-range order. However, in the regime $r_{0,\text{dirty}}^* < r_0 < r_{0,\text{clean}}^*$, following the arguments of Ref. 36, exponentially large droplets have an exponentially large correlation length, which promote quantum Griffiths behavior. Thus, the regime of inhomogeneous nematic order is followed by a quantum Griffiths DW phase, as shown schematically in Fig. 2. The latter is characterized by power-law singularities of thermodynamic and DW-related quantities, with non-universal exponents that depend on r_0 ³⁶. Note that, although our analysis has been restricted to $T = 0$, we expect the smeared transition behavior to persist for small enough temperatures, as the moderate sizes of the relevant droplets can still be smaller than the nematic correlation length.

V. CONCLUDING REMARKS

We showed that even weak disorder fundamentally alters the properties of the Ising-nematic quantum phase transition associated with a mother charge or spin density-wave quantum phase transition. The simultaneous first-order transition of the clean, itinerant system is replaced by an interesting regime that displays inhomogeneous (but long-range) smeared nematic order accompanied by a DW quantum Griffiths phase. The extent and relevance of this regime is controlled by the likelihood of finding isolated droplets of moderate (rather than very large) sizes, which in turn is controlled by the strength of disorder.

These results have important implications for the

understanding of the phase diagrams of copper-based and iron-based superconductors, where an Ising-nematic phase has been argued to emerge from charge and/or spin density-waves. In the case of the iron pnictides, where the Ising-nematic and DW transition lines follow each other closely, these effects are expected to be more pronounced and less ambiguous. Interestingly, elasto-resistance measurements of the nematic susceptibility upon approaching the putative nematic-DW quantum phase transition from high temperatures revealed a weakening of fluctuations and deviation from Curie-Weiss behavior at low temperatures³⁰. This behavior was observed only in compounds with sufficient degree of disorder. We argue that it could be attributed, at least in part, to the onset of long-range nematic order in finite-size droplets. This phenomenon may also help understand the appearance of local inhomogeneous nematic order in NQR measurements in the nominally tetragonal state^{43,44}. Finally, magnetic measurements in Mn-doped BaFe₂As₂, which is significantly less homogeneous than other doped compounds, have been interpreted in terms of a magnetic Griffiths phase^{45,46}. It would be interesting to probe whether local nematic order also emerges in these compounds, simultaneously to the appearance of the reported Griffiths behavior.

ACKNOWLEDGMENTS

We thank A. Chubukov, P. Orth, and J. Schmalian for fruitful discussions. This work was supported by the U.S. Department of Energy, Office of Science, Basic Energy Sciences, under Award number DE-SC0012336.

Appendix A: Derivation of the saddle-point equations for a droplet

We start by rewriting the effective large- N rescaled action for a droplet with linear size L , as given in the main text:

$$S_{\text{eff}}[\psi, \phi] = \frac{1}{L^2} \sum_{\mathbf{q}} \int \frac{d\omega}{2\pi} \left\{ \frac{\phi^2}{2g} - \frac{\psi^2}{2u} + \frac{1}{2} \ln \left[(\chi_{\mathbf{q},\omega}^{-1} + \psi)^2 - \phi^2 \right] \right\} \quad (\text{A1})$$

where ϕ is the Ising-nematic order parameter and ψ is the DW fluctuation field. Here, $\chi_{\mathbf{q},\omega} = (r_0 + \mathbf{q}^2 + \gamma|\omega|)^{-1}$ is the bare DW susceptibility with Landau damping γ and $\mathbf{q} = \frac{2\pi}{L} \mathbf{n}$ is the discretized momentum with $\mathbf{n} = (n_x, n_y)$ and $n_x, n_y \in \mathbb{Z}$. The saddle-point of the effective action is given by setting $\frac{\delta S_{\text{eff}}}{\delta \psi} = \frac{\delta S_{\text{eff}}}{\delta \phi} = 0$, which corresponds

to the following coupled equations,

$$\frac{r - r_0}{u} = \frac{1}{2L^2} \sum_{\mathbf{q}} \int \frac{d\omega}{2\pi} \left(\frac{1}{r + q^2 + \gamma|\omega| - \phi} + \frac{1}{r + q^2 + \gamma|\omega| + \phi} \right) \quad (\text{A2})$$

$$\frac{\phi}{g} = \frac{1}{2L^2} \sum_{\mathbf{q}} \int \frac{d\omega}{2\pi} \left(\frac{1}{r + q^2 + \gamma|\omega| - \phi} \right) \quad (\text{A3})$$

$$- \frac{1}{r + q^2 + \gamma|\omega| + \phi} \right) \quad (\text{A4})$$

where $r \equiv r_0 + \psi$. To tackle the discrete momentum summation, we apply the Poisson summation formula³⁶:

$$\frac{1}{L^d} \sum_{\mathbf{q}} f(\mathbf{q}) = \int \frac{d^d q}{(2\pi)^d} f(\mathbf{q}) + \sum_{\mathbf{n} \neq \mathbf{0}} \int \frac{d^d q}{(2\pi)^d} f(\mathbf{q}) e^{i\mathbf{q} \cdot \mathbf{n}L} \quad (\text{A5})$$

The integrals appearing in the equations above can be evaluated analytically:

$$\int \frac{d^2 q d\omega}{(2\pi)^3} \frac{1}{A + q^2 + \gamma|\omega|} = \int \frac{d^2 q d\omega}{(2\pi)^3} \frac{1}{q^2 + \gamma|\omega|} - \frac{A}{4\pi^2 \gamma} \left[\ln \left(\frac{\Lambda^2}{A} \right) + 1 \right] \quad (\text{A6})$$

and:

$$\int \frac{d^2 q d\omega}{(2\pi)^3} \frac{e^{i\mathbf{q} \cdot \mathbf{n}L}}{A + q^2 + \gamma|\omega|} = \frac{2\sqrt{A}}{L|\mathbf{n}|} K_1 \left(\sqrt{AL} |\mathbf{n}| \right) \quad (\text{A7})$$

where we used the fact that the momentum cutoff is such that $\Lambda^2 \gg r \pm \phi$. We verified that this condition is met for the parameters u and g used in the main text. Defining $\tilde{r}_0 = r_0 + u \int \frac{d^2 q d\omega}{(2\pi)^3} \frac{1}{q^2 + \gamma|\omega|}$, $\tilde{u} = u / (4\pi^2 \gamma)$, and $\tilde{g} = g / (4\pi^2 \gamma)$, we arrive at the equations displayed in the main text:

$$r = \tilde{r}_0 - \tilde{u}r \left(\ln \frac{\Lambda^2}{\sqrt{r^2 - \phi^2}} + 1 - \frac{\phi}{r} \tanh^{-1} \frac{\phi}{r} \right) + \frac{2\pi\tilde{u}}{L^2} (\mathcal{F}[(r - \phi)L^2] + \mathcal{F}[(r + \phi)L^2]) \quad (\text{A8})$$

$$\phi = \phi\tilde{g} \left(\ln \frac{\Lambda^2}{\sqrt{r^2 - \phi^2}} + 1 - \frac{r}{\phi} \tanh^{-1} \frac{\phi}{r} \right) + \frac{2\pi\tilde{g}}{L^2} (\mathcal{F}[(r - \phi)L^2] - \mathcal{F}[(r + \phi)L^2]) \quad (\text{A9})$$

where we defined the function:

$$\mathcal{F}(y) \equiv \frac{1}{\pi} \sum_{\mathbf{n} \neq \mathbf{0}} \frac{\sqrt{y}}{|\mathbf{n}|} K_1(|\mathbf{n}| \sqrt{y}) \quad (\text{A10})$$

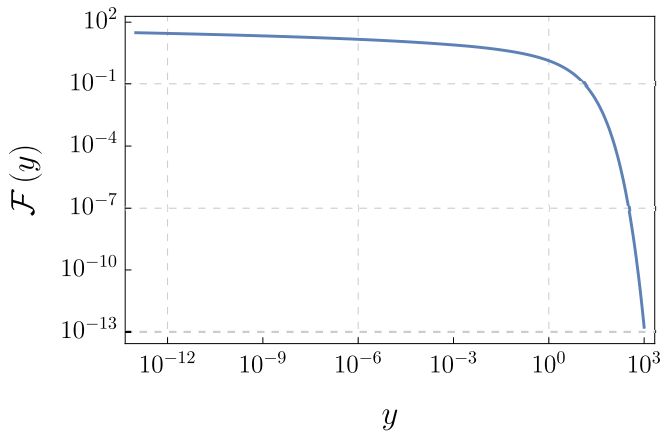


Figure 5. Function $\mathcal{F}(y)$ defined in Eq. (A10).

Note that, for $\phi = 0$, we recover the self-consistent equations of Ref. 36 for an itinerant antiferromagnet. Using the fact that:

$$\frac{\sqrt{y}}{|\mathbf{n}|} K_1(|\mathbf{n}| \sqrt{y}) = \frac{1}{4} \int_0^\infty du u^{-2} e^{-yu - \frac{|\mathbf{n}|^2}{4u}} \quad (\text{A11})$$

we can evaluate the sum and express the function as an integral:

$$\mathcal{F}(y) = \frac{1}{4\pi} \int_0^\infty du u^{-2} e^{-yu} \left[\theta_3^2 \left(0, e^{-\frac{1}{4u}} \right) - 1 \right] \quad (\text{A12})$$

where $\theta_3(a, b)$ is the elliptic theta function. The asymptotic behavior of $\mathcal{F}(y)$ follows from Eqs. (A10) and (A12). For $y \gg 1$, the sum in Eq. (A10) is dominated by the $|\mathbf{n}| = 1$ contribution, and we obtain:

$$\mathcal{F}(y \gg 1) \simeq \frac{2y^{1/4} e^{-\sqrt{y}}}{\sqrt{2\pi}} \quad (\text{A13})$$

For $y \ll 1$, it is more convenient to use the integral representation (A12). Following the same steps as Ref. 36, it follows that the function has a logarithmic divergence:

$$\mathcal{F}(y \ll 1) \simeq -\ln \left(\frac{y e^{\gamma+1}}{4\pi} \right) \quad (\text{A14})$$

where γ is the Euler number. Equations (A8) and (A9) are solved numerically to yield $\phi(r_0, L)$. In the numerical calculation, we use an interpolation function for $\mathcal{F}(y)$ that interpolates between Eq. (A10) with 80×80 terms in the sum and the asymptotic behavior in Eq. (A14). The resulting function is shown in Fig. 5. We checked that the error with respect to the exact function \mathcal{F} is no more than 2%.

Before proceeding, we rederive the solutions of the self-consistent equations in the clean limit (i.e. $L \rightarrow \infty$,

which makes $\mathcal{F}(y) \rightarrow 0$). In this case, the solution of Eqs. (A8) and (A9) shows that r_0 is maximum for $\phi = r$. However, $\phi = r$ implies a DW transition, since the renormalized DW susceptibility is $(r - \phi)^{-1}$. Thus, one has to go back to the action (A1) and consider the possibility of a finite DW order parameter Δ . In the large- N limit, this corresponds to adding the term $\Delta^2 (r - \phi)$ in the action (see for instance⁶). Minimizing with respect to Δ , it is clear that only when $\phi = r$ is that we obtain $\Delta \neq 0$. In this case, the self-consistent equations become:

$$\phi = r_0 - \phi u \left(\ln \frac{\Lambda^2}{2\phi} + 1 \right) + u \Delta^2 \quad (\text{A15})$$

$$\phi = \phi g \left(\ln \frac{\Lambda^2}{2\phi} + 1 \right) + g \Delta^2 \quad (\text{A16})$$

where unimportant constants have been absorbed in Δ . We can now eliminate Δ to find r_0 as function of ϕ :

$$\frac{r_0}{u} = \phi \left(\frac{1}{u} - \frac{1}{g} \right) + 2\phi \left(\ln \frac{\Lambda^2}{2\phi} + 1 \right) \quad (\text{A17})$$

The first-order transition therefore takes place at:

$$\frac{r_{0,\text{clean}}^*}{\Lambda^2} = u \exp \left(\frac{1}{2u} - \frac{1}{2g} \right) \quad (\text{A18})$$

and the jump in ϕ is given by:

$$\phi_{\text{clean}}^* = \frac{r_{0,\text{clean}}^*}{2u} \quad (\text{A19})$$

For the parameters used in the main text, $u = 0.9$ and $g = 0.25u$, we find $\frac{r_{0,\text{clean}}^*}{\Lambda^2} \approx 0.17$ and $\frac{\phi_{\text{clean}}^*}{\Lambda^2} \approx 0.09$. Note that, inside the finite size droplets, $r > \phi$ always. Therefore, we do not need to add the DW field Δ in the self-consistent equations.

Appendix B: Properties of the Ising-nematic order as function of the size of the droplets

Here we discuss how two properties of the Ising-nematic order depend on the size L of the droplet: the character of the transition and the value of the tuning parameter r_0 for which the quantum transition takes place. We consider here the two self-consistent equations (A8) and (A9) with reduced variables $(r_0, r, \phi) \rightarrow (r_0, r, \phi)/\Lambda^2$. Furthermore, the size L of the droplet is measured in units of $1/\Lambda \approx a$, where a is the lattice constant. For convenience, we drop the tilde notation of Eqs. (A8) and (A9) in this section.

The condition for a droplet of size L to undergo a continuous Ising-nematic quantum phase transition is that

$$\left. \frac{dr_0}{d\phi} \right|_{\phi \rightarrow 0} \leq 0 \quad (\text{B1})$$

where r_0 is the tuning parameter. Taking derivatives

with respect to ϕ for the self-consistent equations (A8) and (A9), we find:

$$\frac{1}{u} \frac{dr_0}{d\phi} = \left(\frac{1}{u} + \ln \frac{1}{\sqrt{r^2 - \phi^2}} \right) \frac{dr}{d\phi} - u \tanh^{-1} \frac{\phi}{r} - 2\pi \left\{ \mathcal{F}' [(r + \phi) L^2] \left(1 + \frac{dr}{d\phi} \right) - \mathcal{F}' [(r - \phi) L^2] \left(1 - \frac{dr}{d\phi} \right) \right\} \quad (\text{B2})$$

$$\frac{dr}{d\phi} = \frac{-\frac{1}{g} + \ln \frac{1}{\sqrt{r^2 - \phi^2}} - 2\pi (\mathcal{F}' [(r + \phi) L^2] + \mathcal{F}' [(r - \phi) L^2])}{\tanh^{-1} \left(\frac{\phi}{r} \right) + 2\pi (\mathcal{F}' [(r + \phi) L^2] - \mathcal{F}' [(r - \phi) L^2])} \quad (\text{B3})$$

We can eliminate the logarithms by noting that the second self-consistent equation gives:

$$\frac{1}{g} = \ln \frac{1}{\sqrt{r^2 - \phi^2}} + 1 - \frac{r}{\phi} \tanh^{-1} \left(\frac{\phi}{r} \right) - \frac{2\pi}{\phi L^2} (\mathcal{F} [(r + \phi) L^2] - \mathcal{F} [(r - \phi) L^2]) \quad (\text{B4})$$

Substituting Eq. (B4) in Eqs. (B2)-(B3), and then expanding for small ϕ , we find:

$$\left. \frac{dr_0}{d\phi} \right|_{\phi \rightarrow 0} = \frac{u}{\lambda} \frac{\phi}{3r^{(0)}} \frac{1 - 4\pi\zeta^2 \mathcal{F}'''(\zeta) - 3\lambda [1 + 4\pi\zeta \mathcal{F}''(\zeta)]^2}{1 + 4\pi\zeta \mathcal{F}''(\zeta)} \quad (\text{B5})$$

where we defined, for convenience, $\zeta = r^{(0)} L^2$ and $\frac{1}{\lambda} = \frac{1}{u} + \frac{1}{g}$. From (B5), the condition for a droplet to undergo a continuous Ising-nematic quantum phase transition is:

$$(1 - 3\lambda) - 4\pi\zeta^2 \mathcal{F}'''(\zeta) - 24\pi\lambda\zeta \mathcal{F}''(\zeta) - 48\pi^2\lambda\zeta^2 [\mathcal{F}''(\zeta)]^2 \leq 0 \quad (\text{B6})$$

Note that, here, $r^{(0)}$ is a shorthand notation for $r^{(0)} \equiv r(\phi = 0)$. Thus, its value, as well as the corresponding r_0 , are determined by taking the limit $\phi = 0$ in the self-consistent equations (A8) and (A9):

$$r_0 = ur^{(0)} \left[\frac{1}{u} + 1 - \ln r^{(0)} - \frac{4\pi}{\zeta} \mathcal{F}(\zeta) \right] \quad (\text{B7})$$

$$\frac{1}{g} = -\ln r^{(0)} - 4\pi \mathcal{F}'(\zeta) \quad (\text{B8})$$

Therefore, for given g and u , we can find the critical size of the droplet L_{c1} beyond which it undergoes a first-order transition by solving Eqs. (B6) and (B8) simultaneously:

$$L_{c1}^2 = \zeta_{c1} \exp \left[\frac{1}{g} + 4\pi \mathcal{F}'(\zeta_{c1}) \right] \quad (\text{B9})$$

where ζ_{c1} is the value for which Eq. (B6) satisfies the identity. For the parameters used in the main text, $u = 0.9$ and $g/u = 0.25$, we find $L_{c1}^2 \approx 58$.

Next, we analyze which of the droplets undergoing a second-order phase transition orders at the highest value of the tuning parameter r_0 , i.e. we look for the critical droplet area L_{c2}^2 for which: $\frac{dr_0}{dL^2} = 0$.

Taking the derivative with respect to L^2 on Eqs. (B7) and (B8), we find:

$$\frac{1}{u} \frac{dr_0}{dL^2} = \frac{dr^{(0)}}{dL^2} \left[\frac{1}{\lambda} + 4\pi \mathcal{F}'(r^{(0)} L^2) \right] + \frac{4\pi}{L^4} \mathcal{F}(r^{(0)} L^2) - \frac{4\pi}{L^2} \mathcal{F}'(r^{(0)} L^2) \left(r^{(0)} + L^2 \frac{dr^{(0)}}{dL^2} \right) \quad (\text{B10})$$

$$0 = -\frac{1}{r^{(0)}} \frac{dr^{(0)}}{dL^2} - 4\pi \mathcal{F}''(r^{(0)} L^2) \left(r^{(0)} + L^2 \frac{dr^{(0)}}{dL^2} \right) \quad (\text{B11})$$

Solving for $\frac{dr_0}{dL^2}$, we obtain

$$\frac{dr_0}{dL^2} = \frac{u}{\lambda} \frac{4\pi \exp \left(-\frac{2}{g} - 8\pi \mathcal{F}'(\zeta) \right)}{\zeta + 4\pi\zeta^2 \mathcal{F}''(\zeta)} \times \left\{ \lambda [\mathcal{F}(\zeta) - \zeta \mathcal{F}'(\zeta)] \left[\frac{1}{\zeta} + 4\pi \mathcal{F}''(\zeta) \right] - \zeta \mathcal{F}''(\zeta) \right\} \quad (\text{B12})$$

Therefore, the first droplet that undergoes a continuous Ising-nematic quantum phase transition satisfies

$$[\mathcal{F}(\zeta_{c2}) - \zeta_{c2} \mathcal{F}'(\zeta_{c2})] \left[\frac{1}{\zeta_{c2}} + 4\pi \mathcal{F}''(\zeta_{c2}) \right] = \frac{1}{\lambda} \zeta_{c2} \mathcal{F}''(\zeta_{c2}) \quad (\text{B13})$$

and its area is given by:

$$L_{c2}^2 = \zeta_{c2} \exp \left[\frac{1}{g} + 4\pi \mathcal{F}'(\zeta_{c2}) \right] \quad (\text{B14})$$

Using Eqs. (B7) and (B8), we can find the corresponding value of the control parameter $r_0^*(L_{c2})$ at which this happens:

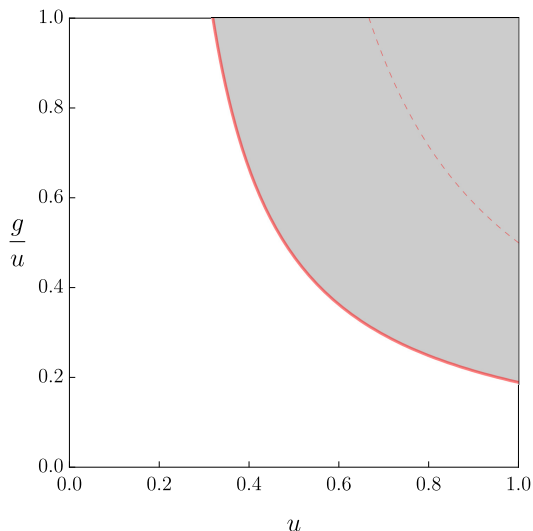


Figure 6. Region in the (u, g) parameter space in which the droplet that orders first does so before the transition of the clean system, i.e. $r_0^*(L_{c2}) > r_{0,\text{clean}}^*$.

$$r_0^*(L_{c2}) = u \exp\left(-\frac{1}{g} - 4\pi\mathcal{F}'(\zeta_{c2})\right) \times \left[\frac{1}{\lambda} + 1 + 4\pi\mathcal{F}'(\zeta_{c2}) - \frac{4\pi}{\zeta_{c2}}\mathcal{F}(\zeta_{c2})\right] \quad (\text{B15})$$

It is instructive to compare it with the value $r_{0,\text{clean}}^*$ for which the first-order transition of the clean system takes place, see Eq. (A18):

$$\frac{r_0^*(L_{c2})}{r_{0,\text{clean}}^*} = \exp\left(-\frac{1}{2\lambda} - 4\pi\mathcal{F}'(\zeta_{c2})\right) \times \left[\frac{1}{\lambda} + 1 + 4\pi\mathcal{F}'(\zeta_{c2}) - \frac{4\pi}{\zeta_{c2}}\mathcal{F}(\zeta_{c2})\right] \quad (\text{B16})$$

For the parameters used in the main text, $u = 0.9$ and $g = 0.25u$, we find $L_{c2}^2 \approx 40$ and $\frac{r_0^*(L_{c2})}{r_{0,\text{clean}}^*} \approx 1.08$. More generally, as a function of the two parameters u and g , there is a wide region in parameter space in which $\frac{r_0^*(L_{c2})}{r_{0,\text{clean}}^*} > 1$, shown as the shaded area in Fig. 6.

Appendix C: Derivation of the probability distribution for the droplets sizes

In this section, we use results from percolation theory to derive the approximate probability distribution function $P(V)$ of finding a finite droplet with “volume” $V = L^2$ that is devoid of impurities. We consider that a local site-impurity completely suppresses both DW and nematic orders. The concentration of impurities is $1 - p$, i.e. the concentration of clean sites is p . From percolation theory, the number of finite-size “clean” clusters (droplets) containing s sites, denoted n_s , satisfies the scaling relation⁴⁰:

$$n_s = \mathcal{N}_0 s^{-\tau} f(s/s_0) \quad (\text{C1})$$

where s_0 , the typical cluster size, diverges at the percolation threshold p_c , τ is a critical exponent, and \mathcal{N}_0 is a normalization constant. The precise form of the scaling function $f(x)$ can only be obtained numerically. However, an often used approximation is an exponential decay:

$$n_s = \mathcal{N}_0 s^{-\tau} \exp(-s/s_0) \quad (\text{C2})$$

Now, the total number of clusters of size s is given by Nn_s , where N is the total number of sites. This implies that the total number of sites that belong to a cluster of size s is Nsn_s . Therefore, the probability $P(s)$ that a given site belong to a cluster of size s is:

$$P(s) \equiv \frac{Nsn_s}{N} = \mathcal{N}_0 s^{1-\tau} \exp(-s/s_0) \quad (\text{C3})$$

The constant \mathcal{N}_0 is given by the normalization condition on n_s :

$$\sum_s sn_s = p - P(p) \quad (\text{C4})$$

where $P(p)$ is the number of sites belonging to the infinite cluster (divided by the total number of sites). Thus, we obtain:

$$\mathcal{N}_0 = \frac{p - P(p)}{\sum_s s^{1-\tau} e^{-s/s_0}} \quad (\text{C5})$$

Importantly, $p - P(p)$ vanishes for both $p = 0$ and $p = 1$, and has a maximum near the percolation threshold p_c . If we are not too far from the percolation threshold, we can then approximate $p - P(p)$ by p_c , as the quantity that changes more strongly upon approaching the percolation threshold is s_0 , which diverges at p_c . We then obtain:

$$P(s) \approx \frac{p_c s^{1-\tau} e^{-s/s_0}}{\sum_s s^{1-\tau} e^{-s/s_0}} \quad (\text{C6})$$

The fact that $P(s)$ is not necessarily normalized to 1 is due to the fact that not all sites belong to a finite cluster.

The relationship between s and the linear size L of the cluster that enters the self-consistent equations (A8) and (A9) is $s = L^2/a^2$, where a is the lattice constant. In our problem, as explained above, L is given in units of the inverse momentum cutoff, $L = \tilde{L}/\Lambda$. Thus, we arrive at $\tilde{L}^2 = s(\Lambda a)^2$, with integer s . For concreteness, in our calculations we set $\Lambda = 1/a$.

-
- ¹ S. A. Kivelson, E. Fradkin, and V. J. Emery, *Nature* **393**, 550 (1998).
- ² M. Vojta, *Advances in Physics* **58**, 699 (2009).
- ³ R. M. Fernandes, A. V. Chubukov, and J. Schmalian, *Nature Physics* **10**, 97 (2014).
- ⁴ C. Xu, M. Müller, and S. Sachdev, *Phys. Rev. B* **78**, 020501 (2008).
- ⁵ C. Fang, H. Yao, W.-F. Tsai, J.-P. Hu, and S. A. Kivelson, *Phys. Rev. B* **77**, 224509 (2008).
- ⁶ R. M. Fernandes, A. V. Chubukov, J. Knolle, I. Eremin, and J. Schmalian, *Phys. Rev. B* **85**, 024534 (2012).
- ⁷ Y. Wang and A. Chubukov, *Phys. Rev. B* **90**, 035149 (2014).
- ⁸ M. Schütt and R. M. Fernandes, *Phys. Rev. Lett.* **115**, 027005 (2015).
- ⁹ L. Nie, A. V. Maharaj, E. Fradkin, and S. A. Kivelson, *Phys. Rev. B* **96**, 085142 (2017).
- ¹⁰ K. Hashimoto, K. Cho, T. Shibauchi, S. Kasahara, Y. Mizukami, R. Katsumata, Y. Tsuruhara, T. Terashima, H. Ikeda, M. A. Tanatar, H. Kitano, N. Salovich, R. W. Giannetta, P. Walmsley, A. Carrington, R. Prozorov, and Y. Matsuda, *Science* **336**, 1554 (2012).
- ¹¹ B. J. Ramshaw, S. E. Sebastian, R. D. McDonald, J. Day, B. S. Tan, Z. Zhu, J. B. Betts, R. Liang, D. A. Bonn, W. N. Hardy, and N. Harrison, *Science* **348**, 317 (2015).
- ¹² I. M. Hayes, R. D. McDonald, N. P. Breznay, T. Helm, P. J. W. Moll, M. Wartenbe, A. Shekhter, and J. G. Analytis, *Nature Physics* **12**, 916 EP (2016).
- ¹³ Y. Schattner, S. Lederer, S. A. Kivelson, and E. Berg, *Phys. Rev. X* **6**, 031028 (2016).
- ¹⁴ Y. Qi and C. Xu, *Phys. Rev. B* **80**, 094402 (2009).
- ¹⁵ A. J. Millis, *Phys. Rev. B* **81**, 035117 (2010).
- ¹⁶ Y. Kamiya, N. Kawashima, and C. D. Batista, *Phys. Rev. B* **84**, 214429 (2011).
- ¹⁷ A. H. Castro Neto, G. Castilla, and B. A. Jones, *Phys. Rev. Lett.* **81**, 3531 (1998).
- ¹⁸ S. Sachdev, C. Buragohain, and M. Vojta, *Science* **286**, 2479 (1999).
- ¹⁹ A. J. Millis, D. K. Morr, and J. Schmalian, *Phys. Rev. Lett.* **87**, 167202 (2001).
- ²⁰ H. Maebashi, K. Miyake, and C. M. Varma, *Phys. Rev. Lett.* **88**, 226403 (2002).
- ²¹ T. Vojta, *Phys. Rev. Lett.* **90**, 107202 (2003).
- ²² V. Dobrosavljević and E. Miranda, *Phys. Rev. Lett.* **94**, 187203 (2005).
- ²³ T. Vojta and J. Schmalian, *Phys. Rev. Lett.* **95**, 237206 (2005).
- ²⁴ H. Alloul, J. Bobroff, M. Gabay, and P. J. Hirschfeld, *Rev. Mod. Phys.* **81**, 45 (2009).
- ²⁵ B. M. Andersen, S. Graser, and P. J. Hirschfeld, *Phys. Rev. Lett.* **105**, 147002 (2010).
- ²⁶ E. C. Andrade, E. Miranda, and V. Dobrosavljević, *Phys. Rev. Lett.* **104**, 236401 (2010).
- ²⁷ E. W. Carlson, K. A. Dahmen, E. Fradkin, and S. A. Kivelson, *Phys. Rev. Lett.* **96**, 097003 (2006).
- ²⁸ K. Lee, S. A. Kivelson, and E.-A. Kim, *Phys. Rev. B* **94**, 014204 (2016).
- ²⁹ V. Mishra and P. J. Hirschfeld, *New Journal of Physics* **18**, 103001 (2016).
- ³⁰ H.-H. Kuo, J.-H. Chu, J. C. Palmstrom, S. A. Kivelson, and I. R. Fisher, *Science* **352**, 958 (2016).
- ³¹ L. Nie, G. Tarjus, and S. A. Kivelson, *Proceedings of the National Academy of Sciences* **111**, 7980 (2014).
- ³² M. Hoyer, R. M. Fernandes, A. Levchenko, and J. Schmalian, *Phys. Rev. B* **93**, 144414 (2016).
- ³³ B. M. McCoy and T. T. Wu, *Phys. Rev.* **176**, 631 (1968).
- ³⁴ R. B. Griffiths, *Phys. Rev. Lett.* **23**, 17 (1969).
- ³⁵ R. Sknepnek and T. Vojta, *Phys. Rev. B* **69**, 174410 (2004).
- ³⁶ T. Vojta and J. Schmalian, *Phys. Rev. B* **72**, 045438 (2005).
- ³⁷ J. A. Hoyos and T. Vojta, *Phys. Rev. B* **74**, 140401 (2006).
- ³⁸ J. A. Hoyos and T. Vojta, *Phys. Rev. Lett.* **100**, 240601 (2008).
- ³⁹ M. Al-Ali, J. A. Hoyos, and T. Vojta, *Phys. Rev. B* **86**, 075119 (2012).
- ⁴⁰ A. Aharony and D. Stauffer, *Introduction to percolation theory* (Taylor & Francis, 2003).
- ⁴¹ T. Vojta, *Journal of Physics A: Mathematical and General* **39**, R143 (2006).
- ⁴² T. Vojta, *Journal of Low Temperature Physics* **161**, 299 (2010).
- ⁴³ G. Lang, H.-J. Grafe, D. Paar, F. Hammerath, K. Manthey, G. Behr, J. Werner, and B. Büchner, *Phys. Rev. Lett.* **104**, 097001 (2010).
- ⁴⁴ A. P. Dioguardi, T. Kissikov, C. H. Lin, K. R. Shirer, M. M. Lawson, H.-J. Grafe, J.-H. Chu, I. R. Fisher, R. M. Fernandes, and N. J. Curro, *Phys. Rev. Lett.* **116**, 107202 (2016).
- ⁴⁵ D. S. Inosov, G. Friemel, J. T. Park, A. C. Walters, Y. Texier, Y. Laplace, J. Bobroff, V. Hinkov, D. L. Sun, Y. Liu, R. Khasanov, K. Sedlak, P. Bourges, Y. Sidis, A. Ivanov, C. T. Lin, T. Keller, and B. Keimer, *Phys. Rev. B* **87**, 224425 (2013).
- ⁴⁶ M. N. Gastiasoro and B. M. Andersen, *Phys. Rev. Lett.* **113**, 067002 (2014).